Terrestrial precise positioning system using carrier phase from burst signals and optically distributed time and frequency reference

Dun, Han; Tiberius, Christian C.J.M.; Diouf, Cherif; Janssen, Gerard J.M.

Important note
To cite this publication, please use the final published version (if applicable).
Please check the document version above.

Terrestrial Precise Positioning System Using Carrier Phase from Burst Signals and Optically Distributed Time and Frequency Reference

Han Dun, Christian C. J. M. Tiberius, Cherif Diouf, *Geoscience and Remote Sensing, Delft University of Technology*

Gerard J. M. Janssen, *Circuits and Systems, Delft University of Technology*

BIOGRAPHIES

Han Dun received his BSc degree in Communication Engineering and MSc degree in Communication and Information Engineering from Shanghai University, China, in 2013 and 2016, respectively. From 2013 to 2016, he also worked at the key laboratory of specialty fiber optics and optical access network in Shanghai University, where he contributed to the real-time optical OFDM-PON. He is currently pursuing his PhD degree in the department of Geoscience and Remote Sensing, Delft University of Technology. His research interests include digital communication theory, wireless localization, and statistical signal processing.

Dr. Christian C. J. M. Tiberius received his PhD degree in 1998 from the Delft University of Technology, Delft, The Netherlands, on recursive data processing for kinematic GPS surveying. He is currently an Associate Professor with the Geoscience and Remote Sensing (GRS) department, Delft University of Technology. His research interest lies in navigation, with GNSS and terrestrial radio positioning, with a focus on high-precision and high-integrity applications.

Dr. Cherif Diouf received a PhD degree in non-linear system modeling applied to VLSI electronic circuits in 2014 from the Université de Bretagne Occidentale (France). He then worked at the Ecole Nationale d'Ingénieurs of Brest on DSP techniques to optimize the performance of optical OFDM communication systems. In 2015, he joined the French Oceanographic institute (Ifremer). As a postdoctoral researcher, he worked on the development of a power-over-fiber prototype to allow extensions of a sea-bed observatory. Recently, he was working as an embedded systems engineer on autonomous floats. In 2018, he joined the SuperGPS research team as a postdoctoral researcher. He is interested in blackbox modeling and DSP techniques, HW/SW implementation and electro-optical systems.

Dr. Gerard J. M. Janssen received the Ph.D. degree from Delft University of Technology, Delft, The Netherlands, in 1998. He is currently an Associate Professor with the Circuits and Systems Group, Delft University of Technology. His research interests include wireless communication, particularly narrowband multiuser detection, digital modulation techniques, channel modeling, diversity techniques, and ultra wideband communications and positioning.

ABSTRACT

Terrestrial positioning systems are being investigated as the complement to the global navigation satellite systems (GNSS), to provide precise and reliable positioning services in a GNSS-challenged environment. In this paper, we present the positioning performance of a ground-based positioning system, in which a multiband OFDM burst is used as a ranging signal to estimate carrier phase, and all transmitters are tightly synchronized by optically distributed time and frequency reference signals. The receiver, like in GNSS, runs on its own clock. An experiment has been carried out in an outdoor living lab environment to demonstrate the flexibility of precise positioning using carrier phase with the proposed ground-based system. During the experiment, the receiver was moved over a trajectory of 17 m forth and back, and acquired the ranging signal for 71 seconds. Without calibrating the different initial phase offsets among the transmitters, we keep the carrier phase cycle ambiguities as float numbers and compute the so called float position solutions. The root mean-squared error (RMSE) of the position solution in East and North direction are 4.22 cm and 4.63 cm, respectively, demonstrating the high-accuracy potential of the proposed burst oriented hybrid optical-wireless terrestrial positioning system.

I. INTRODUCTION

Precise and reliable positioning services have recently become in high demand in various emerging applications, such as autonomous driving and internet-of-things (IoT). Global Navigation Satellite Systems (GNSS) have been widely used and can fulfill the required positioning performance in open areas. However, the performance deteriorates in urban canyons and indoor environments, due to severe multipath and signal blockage. The relatively narrow signal bandwidth and the very low received signal power levels of GNSS signals also make them vulnerable to jamming and spoofing attacks. Therefore, a terrestrial

positioning system has been investigated as a complement to GNSS, which can be deployed regionally to provide precise and reliable terrestrial position, navigation and timing (PNT) services.

Terrestrial GNSS-like systems have recently been proposed as complements and augmentations of GNSS. The pseudolites, which are ground-based, transmit navigation ranging signals as used in GNSS (e.g., a pseudo-random-noise (PRN) code). As timing is crucial for precise positioning, and installation of a highly accurate atomic clock in each pseudolite is prohibitively expensive, synchronization of the pseudolites needs to be arranged otherwise. The synchronization can be achieved based on received wireless signals or based on commonly distributed time and frequency signal using cables. For example, in the Locata system [1, 2], a so-called 'Timeloc' technology is implemented for wireless synchronization. As the performance of the wireless synchronization depends on the wireless channel condition, the location of the pseudolites should be carefully selected to avoid multipath. In [3], to avoid the impact of multipath on clock synchronization, the authors proposed to distribute the time and frequency reference signals (i.e., 1 PPS (pulse-per-second) and 10 MHz) for synchronization through coaxial cables among transmitters in a GNSS-like ground-based system. Due to these cable connections, such a system can only be implemented within a relatively limited area.

The ground-based GNSS-like system uses a narrowband signal for ranging which typically occupies only a few MHz. Based on such a system, the performance of both the wireless synchronization among the pseudolites and positioning is sensitive to multipath. Therefore, an ultra-wideband (UWB) system [4], which uses a much larger signal bandwidth and thus offers a higher time resolution, has recently been proposed for positioning, Nevertheless, all transmitters need to be synchronized, for example, based on round-trip time estimation [5].

In [6], we proposed a hybrid optical-wireless terrestrial positioning system, which can support a large signal bandwidth (e.g., 160-320 MHz). The radio transmitters (i.e., pseudolites) are synchronized with common reference signals (i.e., 10 MHz and 1 PPS) generated by a central atomic clock and distributed to each radio transmitter through an optical telecommunication infrastructure using the White Rabbit precision time protocol (WR-PTP) [7, 8]. As the system is developed under the SuperGPS project (funded by the Dutch Research Council, NWO), the prototype system is referred to as the "SuperGPS system" in this paper. Using a relatively large radio signal bandwidth in this system improves the resolvability of reflections in a multipath channel. In addition, using the optically distributed time and frequency reference signals through the existing optical communication infrastructure provides flexibility to expand the system over a large area, and the synchronization, in case of wireless distribution of the reference signals among the transmitters, is not affected by multipath which is prominently present in an urban area.

To be spectrum efficient and adaptable to existing telecommunication networks, a multiband orthogonal frequency division multiplexing (OFDM) signal, which occupies a total of 160 MHz of virtual bandwidth, is used as a ranging signal in the system. OFDM has been adopted in various telecommunication systems which also have been exploited as signal-of-opportunities for positioning, such as in Wi-Fi [9], 4G/5G [10, 11, 12, 13], and DVB-T [14]. As indicated in [15], only a few signal bands, sparsely located in the available signal spectrum, are needed to create a large virtual signal bandwidth to achieve a high ranging precision.

In a terrestrial positioning system, the radio transmitters are generally fixed and static. As the radio receiver (e.g., carried by pedestrians and ground-based vehicles) moves relatively slowly, it is unnecessary to continuously transmit the ranging signal for tracking. Therefore, in the SuperGPS system, the ranging signal is transmitted as low duty-cycle bursts within a time division multiplexing (TDM) scheme, which largely improves the time efficiency and leaves most of the spectral resources to other telecommunication applications.

The time delay and the carrier phase are the most common observables for positioning. They can be jointly estimated from the ranging signal through maximum likelihood (ML) estimation in a stepwise manner [16, 17]. Compared with the propagation time delay, the carrier phase is much more spectrum efficient in providing an equivalent ranging precision, because of the short wavelength of the central carrier. However, the phase cycle ambiguity should be resolved, either as a float number or fixed into an integer number, in the positioning model. In this paper, we assess the positioning performance of the hybrid optical-wireless SuperGPS terrestrial positioning system, based on the carrier phase estimated through the OFDM burst ranging signals.

This paper is organized as follows. First, the signal structure and the received signal model, as well as the impact of a sampling frequency offset and a carrier frequency offset are provided in section II.. Then, a step-wise carrier phase estimation and tracking of the multiband OFDM signal is introduced in section III.. In section IV., a positioning model is derived for an asynchronous system, only based on the carrier phase. Afterwards, in section V., results from an outdoor experiment are presented to demonstrate a centimeter level positioning accuracy with a moving receiver. Lastly, conclusions are drawn in section VI..

Notation:

The superscript and subscript of a variable (e.g., φ_r^i) generally denote the index of the transmitter (e.g., i) and the receiver (e.g., r), respectively. Uppercase boldface letters (e.g., $\boldsymbol{G}$) are used for matrices, and lowercase boldface letters (e.g., $\boldsymbol{g}$) denote

column vectors. $[\cdot]_{i,j}$ denotes the element in the i-th row and the j-th column of a matrix. $\mathcal{I}_N$ stands for an identity matrix of size N. $\mathbf{1}_N$ denote a N-by-1 vector of ones. $(\cdot)^{\mathrm{T}}$, $(\cdot)^{*}$ and $(\cdot)^{\mathrm{H}}$ denote transposition, conjugate and Hermitian operation, respectively. j denotes the imaginary unit. $\boldsymbol{A}$ and $\boldsymbol{u}$ denote a design matrix and a vector which contains unknown parameters, respectively.

II.   SIGNAL MODEL

1.   Received Multiband OFDM Burst

A burst signal packet, which consists of three multiband OFDM pilot symbols (i.e., training symbol), is currently implemented for ranging in the SuperGPS system as shown in Fig. 1(a). The first two symbols are the normal pilot symbols, which are known to the receiver and will be used for synchronization and channel estimation. A PRN sequence, as an example, is modulated on all subcarriers in each signal band, and it is identical for all transmitters. The last symbol is a shortened Moose's pilot symbol [18], in which only every other subcarrier is used in an OFDM symbol, so that the first half of the symbol in time is equal to the second half, excluding the cyclic prefix (CP). A Gold sequence is modulated on the activated subcarriers in the Moose's symbol. Each transmitter modulates a unique Gold sequence as an ID to allow for the identification by the receiver. In addition, as an TDM scheme is applied in the current system, the burst ranging signal packet is transmitted with a period of T_D, and different transmitters occupy different time slots for the transmission (in the prototype system we have 6 transmitters).
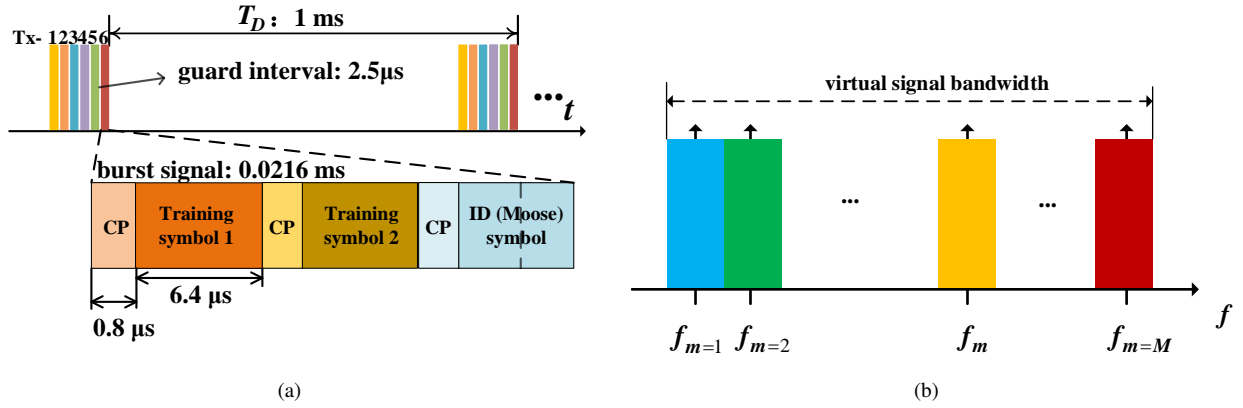

Figure 1: (a) Each transmitter transmits a burst ranging signal in a time-division scheme with a period of T_D. Each burst ranging signal packet consists of three OFDM symbols, (b) spectrum of multiband OFDM signal (in baseband), which consists of M available signal bands and N subcarriers in each signal band.

In addition, as shown in Fig. 1(b), there are M available bands in the allocated signal spectrum that can be used for positioning. Given a medium total signal bandwidth (e.g., 100-200 MHz), all signal bands can be received simultaneously through a single RF front-end and analog-to-digital converter (ADC). To preserve the characteristics of the shortened Moose's symbol, the number of subcarriers N in each signal band should be an even number.

In order to properly track the carrier phase for positioning without cycle-slips, the transmission period T_D for each transmitter should be carefully determined. The faster the receiver is moving, the shorter the transmission period shall be, in order to avoid the occurrence of cycle-slips in the phase. For example, given a central frequency of 3960 MHz (as in our system), and a receiver moving with a speed of 80 km/h (i.e., 22.22 m/s), the maximum Doppler frequency offset is about 293.51 Hz. Considering a transmission period T_D of 1 millisecond, the maximum phase rotation will be already about 0.29 cycle within this period.

Given the baseband OFDM signal $s_{bb,m}(t)$ for the m-th signal band, the passband multiband OFDM signal modulated on the carrier f_c is given by

$$s_{pb}(t) = \Re \left\{ \underbrace{\sum_m s_{bb,m}(t) \exp(j2\pi f_m t)}_{s_{bb}(t)} \exp\left(j2\pi f_c t + \vartheta_t\right) \right\}, \tag{1}$$

in which $\Re$ denotes the real part of a complex value, f_m denotes the central frequency of the m-th signal bands, f_c denotes the central frequency of the entire multiband OFDM signal, ϑ_t denotes the initial phase offset at the transmitter, the subscript 'bb'

and 'pb' denote 'baseband' and 'passband', respectively.

Apart from the Doppler frequency offset due to receiver motion, a frequency offset will be introduced by the receiver itself as it runs on its own clock, which is not synchronized to the time-frequency reference of the transmitters. In an asynchronous system, due to the sampling frequency offset (SFO) $\Delta f_s(t)$ and the carrier frequency offset (CFO) $\Delta f_c(t)$, the sampling frequency f_s' and the central frequency f_c' generated by the receiver, are given by

$$f_s'(t) = (1 + \eta(t)) f_s = f_s + \Delta f_s(t), \quad f_c'(t) = (1 + \eta(t)) f_c = f_c + \Delta f_c(t), \tag{2}$$

where f_s and f_c respectively denote the sampling frequency and the central frequency generated in the transmitter, and $\eta(t)$ denotes the normalized frequency offset

$$\eta(t) = \frac{\Delta f_s(t)}{f_s} = \frac{\Delta f_c(t)}{f_c}. \tag{3}$$

Note that the frequency offset is defined with respect to the frequency generated by the transmitter. Therefore, the argument t is not present in the frequencies generated by the transmitter.

As the normalized frequency offset η is typically small (e.g., a few ppm (part-per-million)), one can have

$$T_s'(t) = \frac{1}{(1 + \eta(t)) f_s} \approx (1 - \eta(t)) T_s, \tag{4}$$

where T_s and T_s' denotes the sample interval generated in the transmitter and receiver, respectively. In this paper, all signal bands are assumed to be acquired through a single RF front-end, thus the sampling frequency should cover the entire virtual signal bandwidth B. As shown in Fig.1(b), considering M signal bands and N subcarrier in each signal band, one has

$$T_s = \frac{1}{B} = \frac{1}{MN\Delta f}, \quad \Delta f = \frac{1}{NMT_s}, \tag{5}$$

where Δf denotes the subcarrier spacing.

At the receiver, the passband signal $s_{pb}(t)$, perturbed by the channel and the noise, is down-converted to baseband with a locally generated carrier f_c'. Thus, the received baseband signal is written as

$$r_{bb}(t) = 2\mathcal{F}_{\mathrm{L}} \left\{ (s_{pb}(t) * h(t)) \cos \left(2\pi f_c t + \vartheta_a(t) + \vartheta_r \right) \right\} - j2\mathcal{F}_{\mathrm{L}} \left\{ (s_{pb}(t) * h(t)) \sin \left(2\pi f_c t + \vartheta_a(t) + \vartheta_r \right) \right\}, \tag{6}$$

where $\mathcal{F}_{\mathrm{L}}$ denotes a low-pass filter operator, $*$ denotes convolution, $h(t)$ denotes the channel impulse response, ϑ_r denotes the initial phase offset at the receiver, and $\vartheta_a(t)$ denotes the accumulated phase offset, given by

$$\vartheta_a(t) = 2\pi \int_{t_0}^{t} \Delta f_c(\nu) \mathrm{d}\nu. \tag{7}$$

To analyse the impact of the frequency offset on the time delay and the carrier phase, and to keep the derivation mathematically manageable, a direct or Line-of-Sight (LoS) path channel is considered,

$$h(t) = \alpha \delta(t - \tau),$$

where α denotes the propagation gain of the LoS path, and τ denotes the LoS propagation time delay. Then, the received signal (6) is rewritten by

$$r_{bb}(t) = \alpha s_{bb}(t - \tau) \exp(-j(2\pi f_c \tau + \vartheta_a(t))) \exp(j(\vartheta_t - \vartheta_r)), \tag{8}$$

where ϑ_t denotes the initial carrier phase offset in the transmitter as used in (1).

As the CFO and SFO are assumed to be invariant at least within one OFDM symbol, with a duration typically in the order of microseconds, the sample interval $T_s' \approx (1 - \eta) T_s$ is presented without argument t in the following derivations. After the ADC, the discrete received baseband OFDM symbol from the k-th packet with NM samples is given by

$$\begin{aligned} r_{bb}[n; \Delta t_k] &= \alpha s_{bb}(nT_s' - \tau - \tau_a(\Delta t_k)) \exp\left(-j(2\pi f_c \tau + \vartheta_a(\Delta t_k) + 2\pi \Delta f_c n T_s')\right) \exp(j(\vartheta_t - \vartheta_r)), \\ &= r_{bb}^{(1)}[n; \Delta t_k] r_{bb}^{(2)}[n; \Delta t_k], \quad n = N_g, \, \ldots, \, N_g + NM - 1, \end{aligned} \tag{9}$$

where Δt_k is the elapsed time between the 1-st received packet and the k-th packet, and

$$r_{bb}^{(1)}[n; \Delta t_k] = \sum_m \sum_i c_{i,m} \exp(-j2\pi(f_i + f_m)(\tau + \tau_a(\Delta t_k))) \exp\left(-j2\pi(f_i + f_m)(n - N_g)T_s'\right),$$

$$r_{bb}^{(2)}[n; \Delta t_k] = \alpha \exp(-j2\pi f_c \tau) \exp\left(-j(\vartheta_a(\Delta t_k) + 2\pi\Delta f_c(n - N_g)T_s')\right) \exp(j(\vartheta_t - \vartheta_r)),$$

(10)

with

$$\tau_a(\Delta t_k) = \sum_{v=0}^{\Delta t_k/T_s - 1} \eta[v]T_s,$$

and N is assumed to be an even number, $f_i = i\Delta f$ denotes the frequency of the i-th subcarrier in each band, n denotes the sample index in the current symbol, $c_{i,m}$ denotes the pilot data modulated on the i-th subcarrier in the m-th band, N_g denotes the number of samples in the cyclic prefix and $\tau_a(\Delta t_k)$ denotes the accumulated time offset due to the SFO.

2. Coarse Carrier Frequency Offset Estimation

In (9), the discrete received signal has been split into two parts (i.e., $r_{bb}^{(1)}[n; \Delta t_k]$ and $r_{bb}^{(2)}[n; \Delta t_k]$).We first analyse the term $r_{bb}^{(1)}[n; \Delta t_k]$ in (9), and show that the first half of the shortened Moose's symbol will be approximately the same as the second half, and the impact of CFO will be reflected in the term $r_{bb}^{(2)}[n, \Delta t_k]$. Finally, based on the correlation between the first half of the symbol and the second half, the CFO is estimated [19].

Using the second half of the shortened Moose's symbol with $n = N_g, \ldots, N_g + NM/2 - 1$, we have

$$r_{bb}^{(1)}[n + NM/2; \Delta t_k] = \sum_m \sum_{i=\text{even}} c_{i,m} \exp(-j2\pi(f_i + f_m)(\tau + \tau_a(\Delta t_k))) \exp\left(-j2\pi(f_i + f_m)(n - N_g)T_s'\right)$$

$$\exp\left(-j2\pi(f_i + f_m)(NM/2)(1 - \eta)T_s\right)$$

$$= \sum_m \sum_{i=\text{even}} c_{i,m} \exp(-j2\pi(f_i + f_m)(\tau + \tau_a(\Delta t_k))) \exp\left(-j2\pi(f_i + f_m)(n - N_g)T_s'\right) \exp\left(-j(i + mN)\pi(1 - \eta)\right) \quad (11)$$

$$\approx \sum_m \sum_{i=\text{even}} c_{i,m} \exp(-j2\pi(f_i + f_m)(\tau + \tau_a(\Delta t_k))) \exp\left(-j2\pi(f_i + f_m)(n - N_g)T_s'\right) = r_{bb}^{(1)}[n; \Delta t_k].$$

As only every other subcarrier is used in the shortened Moose's symbol, i is an even number in (11). Also because the normalized frequency offset η is typically small and $i + mN$ is an even number, the term $r_{bb}^{(1)}[n; \Delta t_k]$ is approximately equal to $r_{bb}^{(1)}[n + NM/2; \Delta t_k]$. To remove the common phase offset in $r_{bb}^{(2)}[n; \Delta t_k]$ and $r_{bb}^{(2)}[n + NM/2; \Delta t_k]$, one has

$$r_{bb}^*[n; \Delta t_k]r_{bb}[n + N/2; \Delta t_k] = |r_{bb}[n; \Delta t_k]|^2 \exp\left(-j2\pi\Delta f_c \frac{NM}{2}(1 - \eta)T_s\right)$$

$$\approx |r_{bb}[n; \Delta t_k]|^2 \exp\left(-j2\pi\Delta f_c \frac{NM}{2}T_s\right)$$

(12)

$$= |r_{bb}[n; \Delta t_k]|^2 \exp\left(-j\pi\Delta f_c NMT_s\right).$$

Therefore, using the shortened Moose's symbol, the CFO can be estimated by

$$\Delta \check{f}_c(\Delta t_k) = -\frac{\check{\psi}}{\pi NMT_s}, \quad \check{\psi} = \arg\left\{\sum_{n=N_g}^{NM/2+N_g-1} r_{bb}^*[n; \Delta t_k]r_{bb}[n + NM/2; \Delta t_k]\right\},$$

(13)

where the check-symbol (i.e.,˘) is used to denote the coarse estimate.

The CFO will cause a change in carrier phase as time elapses, even when the receiver is static. As a burst signal is used for ranging and positioning, if the carrier phase rotates more than one cycle within the transmission period of the burst ranging signal, a cycle-slip will be introduced in the carrier phase measurement. To reduce the extra phase rotation due to CFO, one can

estimate and compensate the CFO based on the shortened Moose's symbol with (13),

$$\begin{aligned}
\check{r}_{bb}[n; \Delta t_k] &= r_{bb}[n; \Delta t_k] \exp(j\check{\vartheta}_a(\Delta t_k)) \\
&= \alpha s_{bb}[nT'_s - \tau - \tau_a(\Delta t_k)] \exp\left(-j\left(2\pi f_c \tau + \tilde{\vartheta}_a(\Delta t_k)\right)\right) \exp(j(\vartheta_t - \vartheta_r))
\end{aligned} \tag{14}$$

where

$$\tilde{\vartheta}_a(\Delta t_k) = \vartheta_a(\Delta t_k) - \check{\vartheta}_a(\Delta t_k) = 2\pi \int_{\nu=0}^{\nu=\Delta t_k} \left(\Delta f_c(\nu) - \Delta \check{f}_c(\nu)\right) d\nu. \tag{15}$$

The extra rotation of the carrier phase $\tilde{\vartheta}_a(\Delta t_k)$ caused by the residual CFO, is referred to as the *clock error* in this paper, and will be estimated along with the position coordinates in a positioning model introduced in section IV.

Generally, the CFO can be assumed to be relatively stable for a certain period (e.g., for a few seconds), and the CFO estimate for the compensation does not need to be updated for every ranging signal packet (i.e., with an update rate of T_D). The coarse CFO can be determined by the Moose's symbol from all received signal packets within a certain period together to improve the precision.

As shown in (13), the CFO is estimated in the range of $\pm \Delta f$ (over a period of $MNT_s/2$). Later, the clock error $\tilde{\vartheta}_a(\Delta t_k)$, computed along with the position solution in a positioning model, which will be introduced in section IV., can also be used for CFO estimation within a range of $\pm 1/2T_D$ (i.e., over a period of T_D). As the transmission period T_D is much longer than the OFDM symbol time, the CFO estimated based on the clock error can provide a much finer frequency range than the one based on the shortened Moose's symbol. Therefore, in this paper, CFO estimation based on the shortened Moose's symbol is referred to as *coarse* CFO estimation (the estimate is denoted by $\Delta \check{f}_c$), and the one based on the positioning model is referred to as *fine* CFO estimation (the estimate will be denoted by $\Delta \hat{\tilde{f}}_c$).

III. CARRIER PHASE

In this section, the propagation time delay and the carrier phase will be jointly estimated based on the ML method. This procedure is implemented in a step-wise manner to reduce the computational complexity.

To simplify notation, we drop the variable of the elapsed time Δt_k in the following derivations. Given an L-path channel, the *sampled* complex channel impulse response [20] is given by,

$$h(n) = \sum_{l=1}^{L} x_l \delta\left(nT_s - (\tau_l + \tau_{a,l})\right), \quad x_l = \alpha_l \exp\left(-j(2\pi f_c \tau_l + \tilde{\vartheta}_{a,l})\right), \tag{16}$$

where τ_l denotes the propagation delay of the l-th path, x_l stands for the complex gain, α_l denotes the modulus of x_l and is a real number, $\tau_{a,l}$ and $\tilde{\vartheta}_{a,l}$ denote the clock error in time delay and carrier phase for the l-th path, respectively. The phase in the complex gain x_l, which contains the ambiguous ranging information, is defined as *carrier phase* in this paper. By default, $l = 1$ represents the LoS path.

After packet synchronization and FFT, the channel frequency response $\boldsymbol{H}$ is estimated from the first two pilot symbols of the multiband OFDM signal that consists of M signal bands and N subcarriers in each band. Now the measurement model is given by

$$\bar{\boldsymbol{H}} = \mathcal{F}\{h(n)\} = \begin{bmatrix} \boldsymbol{a}_1(\tau_1 + \tau_{a,1}) & \boldsymbol{a}_1(\tau_2 + \tau_{a,2}) & \cdots & \boldsymbol{a}_1(\tau_L + \tau_{a,L}) \\ \vdots & \vdots & & \vdots \\ \boldsymbol{a}_M(\tau_1 + \tau_{a,1}) & \boldsymbol{a}_M(\tau_2 + \tau_{a,2}) & \cdots & \boldsymbol{a}_M(\tau_L + \tau_{a,L}) \end{bmatrix} \begin{bmatrix} \alpha_1 \exp\left(-j(2\pi f_c \tau_1 + \tilde{\vartheta}_{a,1})\right) \\ \alpha_2 \exp\left(-j(2\pi f_c \tau_2 + \tilde{\vartheta}_{a,2})\right) \\ \vdots \\ \alpha_L \exp\left(-j(2\pi f_c \tau_L + \tilde{\vartheta}_{a,L})\right) \end{bmatrix} = \boldsymbol{A}(\boldsymbol{\tau})\boldsymbol{x} \tag{17}$$

where

$$[\boldsymbol{a}_m(\tau_l + \tau_{a,l})]_i = \exp\left(-j2\pi(f_m + f_i)(\tau_l + \tau_{a,l})\right), \quad x_l = \alpha_l \exp\left(-j(2\pi f_c \tau_l + \tilde{\vartheta}_{a,l})\right),$$

$$\boldsymbol{a}_m(\tau_l + \tau_{a,l}) \in \mathbb{C}^{N \times 1}, \quad \boldsymbol{A}(\boldsymbol{\tau}) \in \mathbb{C}^{MN \times L}, \quad \boldsymbol{x} \in \mathbb{C}^{L \times 1},$$

$\mathcal{F}$ denotes the FFT. The carrier phase of the LoS path is of interest for positioning. In (17), except for the complex gain $\boldsymbol{x}$, the unknown parameter is also present in the design matrix $A(\boldsymbol{\tau})$, due to the delay $\boldsymbol{\tau}$.

The maximum likelihood (ML) method can be applied to jointly estimate the time delay and the complex gain. Assuming complex Gaussian noise with zero mean in the channel frequency response $\underline{\boldsymbol{H}}$, we have

$$\underline{\boldsymbol{H}} \sim \mathcal{CN}\left(\bar{\boldsymbol{H}}, \, \boldsymbol{Q_H}\right), \quad \boldsymbol{Q_H} = \sigma^2 \boldsymbol{\mathcal{I}}_{NM}, \tag{18}$$

with mean $\bar{\boldsymbol{H}}$ and variance matrix $\boldsymbol{Q_H}$. The time delay and the carrier phase can now be jointly estimated through minimizing the following cost function

$$\hat{\boldsymbol{\tau}}, \hat{\boldsymbol{x}} = \arg\min_{\boldsymbol{\tau}, \boldsymbol{x}} ||\boldsymbol{H} - A(\boldsymbol{\tau})\boldsymbol{x}||^2_{\boldsymbol{Q_H^{-1}}}. \tag{19}$$

If $\hat{\boldsymbol{\tau}}$ and $\hat{\boldsymbol{x}}$ are the global minimizers of (19), $\hat{\boldsymbol{x}}$ must satisfy [17]

$$\hat{\boldsymbol{x}} = \left(A(\hat{\boldsymbol{\tau}})^{\mathrm{H}} \boldsymbol{Q_H^{-1}} A(\hat{\boldsymbol{\tau}})\right)^{-1} A(\hat{\boldsymbol{\tau}})^{\mathrm{H}} \boldsymbol{Q_H^{-1}} \boldsymbol{H}, \tag{20}$$

where the variance matrix $\boldsymbol{Q_H}$ is a diagonal matrix as defined in (18). In order to construct the design matrix $A(\boldsymbol{\tau})$, the time delay can be estimated by [17, 21]

$$\hat{\boldsymbol{\tau}} = \arg\min_{\boldsymbol{\tau}} \left\| P^{\perp}_{A(\boldsymbol{\tau})} \boldsymbol{H} \right\|^2_{\boldsymbol{Q_H^{-1}}} = \arg\min \frac{1}{\sigma^2} \mathrm{tr}\left\{ P^{\perp}_{A(\boldsymbol{\tau})} \boldsymbol{H}\boldsymbol{H}^{\mathrm{H}} \right\}, \tag{21}$$

where

$$P^{\perp}_{A(\boldsymbol{\tau})} = \boldsymbol{\mathcal{I}}_{NM_a} - P_{A(\boldsymbol{\tau})}, \quad P_{A(\boldsymbol{\tau})} = A(\boldsymbol{\tau}) \left(A(\boldsymbol{\tau})^{\mathrm{H}} \boldsymbol{Q_H^{-1}} A(\boldsymbol{\tau})\right)^{-1} A(\boldsymbol{\tau})^{\mathrm{H}} \boldsymbol{Q_H^{-1}}.$$

Afterwards, the carrier phase is determined by computing the angle of the LoS complex gain,

$$\phi = \arg\left(x_1\right). \tag{22}$$

Thus, one can first estimate the time delay $\hat{\boldsymbol{\tau}}$, construct the design matrix $A(\hat{\boldsymbol{\tau}})$, and then estimate the complex gain, from which the carrier phase of the LoS path can be computed for positioning [16].

To unbiasedly estimate the time delay and the complex gain, one should first determine the number of paths (i.e., L) in the multipath channel, and then consider both the LoS and all reflections in the design matrix $A(\boldsymbol{\tau})$ in (21) and (20). However, considerable computational resources are required to obtain the unbiased solution. In the current system, a 160 MHz signal bandwidth is used for ranging, which largely improves the resolvability of multipath. Therefore, we can simply reduce the dimension of the design matrix to 1 (i.e., only one column in (17)), which means that only the LoS path is considered in the model. Consequently, the computational complexity can be largely reduced, but the time delay and the carrier phase become biased. For the carrier phase, the resulting bias is generally much smaller that one cycle. Due to the small wavelength of the central carrier (in our case 7.6 cm), the bias, which propagates into the position solution, is typically acceptable for the user.

As the carrier phase ϕ from (22) varies from $-\pi$ and π and is ambiguous, each carrier phase estimate carries its own *integer phase cycle ambiguity*. Directly using the carrier phase estimates in the positioning model will lead to a rank deficiency, because of too many unknown parameters. Therefore, the carrier phase ϕ should be properly unwrapped, so that only an initial integer carrier phase ambiguity is preserved, and the change of the carrier phase cycle due to the movement of the receiver and the residual CFO will be absorbed in the unwrapped carrier phase measurements φ.

IV. POSITIONING IN ASYNCHRONOUS SYSTEM

In this section, a positioning model is presented only based on the carrier phase. All transmitters are synchronized through the optically distributed time and frequency reference signals, but the receiver runs on its own clock.

1. Positioning Model

Unlike in GNSS where the medium earth orbit (MEO) satellites are constantly moving, the radio transmitters in a terrestrial positioning system are fixed and static. In order to use carrier phase for positioning, *receiver motion* is *required* to create a change in the positioning geometry. Therefore, the change of the carrier phase estimates is caused by the change in the clock error and the Doppler frequency offset (movement, i.e., change in position).

The properly unwrapped carrier phase estimates in units of length obtained from an asynchronous system is given by

$$\underline{\varphi}_r^i(t) = \rho_r^i(t) + c\tau_{h,r} + \lambda \left(\frac{\tilde{\vartheta}_a(t) + \vartheta^i - \vartheta_r}{2\pi} - N_r^i \right) + \underline{e}_r^i(t), \tag{23}$$

where the superscript i denotes the index of the transmitter, λ denotes the wavelength of the central carrier at f_c, $\rho_r^i(t)$ denotes the propagation distance between the i-th transmitter and the receiver, N_r^i denotes the integer carrier phase cycle ambiguity, $\tau_{h,r}$ denotes the sum of the hardware delay in the transmitter and the receiver, $\tilde{\vartheta}_a(t)$ denotes the clock error introduced by the residual CFO, ϑ^i denotes the initial phase offset from the i-th transmitter (i.e., ϑ_t used in section II.). In addition, $e_r^i(t)$ contains the thermal noise and likely also includes an additional multipath error as not all reflections are considered in (20).

As every transmitter-receiver link carries its own integer carrier phase cycle ambiguity, measurements taken from at least two different time epochs with a change in geometry are required in the positioning model. Moreover, the carrier phase cycle ambiguities N_r^i are linearly dependent on the clock error $\tilde{\vartheta}_a(t)$ (expressed in radians), which is a receiver-dependent and time-variant parameter. Therefore, the design matrix of the positioning model is still not a full-rank matrix. It becomes a rank-defect least-squares (LS) problem, which, however, can be solved by applying the $\mathcal{S}$-system theory [22, 23]. The phase ambiguities and the clock error cannot be separated, only their combination is estimable. We can select one of the transmitters as the pivot transmitter, and combine the clock error and the phase ambiguity of the pivot transmitter as one unknown parameter. Then, the carrier phase ambiguities for the rest of the transmitters can be estimated as the difference with respect to the ambiguity of the pivot transmitter. Therefore, the positioning model based on the carrier phase obtained at two different epochs from K transmitters is given by

$$\begin{bmatrix} \boldsymbol{\varphi}_r(t_1) \\ \boldsymbol{\varphi}_r(t_2) \end{bmatrix} = \begin{bmatrix} \boldsymbol{G}_r(t_1) & \boldsymbol{0} & -\lambda\boldsymbol{1}_K & \boldsymbol{0} & \boldsymbol{\Omega} \\ \boldsymbol{0} & \boldsymbol{G}_r(t_2) & \boldsymbol{0} & -\lambda\boldsymbol{1}_K & \boldsymbol{\Omega} \end{bmatrix} \begin{bmatrix} \Delta x(t_1) \\ \Delta x(t_2) \\ \tilde{\delta}_r^p(t_1) \\ \tilde{\delta}_r^p(t_2) \\ \tilde{\boldsymbol{N}}_r \end{bmatrix} = \boldsymbol{Au}, \tag{24}$$

where

$$\begin{aligned}
\boldsymbol{\varphi}_r(t) &= \begin{bmatrix} \varphi_r^1(t) & \cdots & \varphi_r^K(t) \end{bmatrix}^{\mathrm{T}}, \\
\boldsymbol{G}_r(t) &= \begin{bmatrix} \boldsymbol{g}_r^1(t)^{\mathrm{T}} & \cdots & \boldsymbol{g}_r^K(t)^{\mathrm{T}} \end{bmatrix}^{\mathrm{T}}, \\
\tilde{\delta}_r^p(t) &= N_r^p - \frac{\tilde{\vartheta}_a(t) + \vartheta^p - \vartheta_r}{2\pi} - \frac{c\tau_{h,r}}{\lambda}, \\
\begin{bmatrix} \tilde{\boldsymbol{N}}_r \end{bmatrix}_i &= N_r^i - N_r^p + \frac{\vartheta^p - \vartheta^i}{2\pi}, \quad i \neq p, \text{ and } i = 1, \dots, K,
\end{aligned} \tag{25}$$

and $\Delta x(t)$ contains the unknown coordinates of the receiver at time instant t, $\boldsymbol{g}_r^i(t)$ is the transmitter-receiver geometric unit direction vector, superscript p denotes the pivot transmitter, $\boldsymbol{\Omega}$ denotes a matrix $\lambda\boldsymbol{\mathcal{I}}_K$ with its first column removed (hence $\boldsymbol{\Omega} \in \mathbb{R}^{K \times (K-1)}$). To obtain the solution of (24), linearization based on Taylor expansion and Gauss-Newton iteration are applied here to solve this nonlinear model. As $\tilde{\delta}_r^p(t)$ contains the time-variant clock error $\tilde{\vartheta}_a(t)$, it could be used to analyze the behavior of the clock, and potentially be used as well for synchronization. However, as $\tilde{\delta}_r^p(t)$ also contains the carrier phase ambiguity of the pivot transmitter and the hardware delay, $\tilde{\delta}_r^p(t)$ in (25) is referred to as the *relative clock error* in this paper.

Based on the positioning model (24), the formal error of the solution can be determined by

$$\boldsymbol{Q}_{\hat{\boldsymbol{u}}} = \left(\boldsymbol{A}^{\mathrm{T}} \boldsymbol{Q}_\varphi^{-1} \boldsymbol{A} \right)^{-1}, \tag{26}$$

where $\boldsymbol{Q}_\varphi$ denotes the variance matrix of the carrier phase measurements. According to [16], the variance of the carrier phase (with unit of m^2) can be determined by

$$\sigma_\varphi^2 \approx \frac{1}{2NM\mathrm{SNR}} \left(\frac{\lambda}{2\pi} \right)^2, \tag{27}$$

where SNR denotes the signal-to-noise ratio (SNR).

Note that due to the initial carrier phase offset and the hardware delay, the carrier phase ambiguities in $\tilde{N}_r$ are no longer integer parameters. Without a calibration or correction, the carrier phase ambiguities should be treated as constant float numbers, and one will consequently obtain a so-called float solution. However, as the transmitters in a terrestrial positioning system generally are deployed densely in a certain area, with rather short distances to the receiver, a relatively small displacement of the receiver (e.g., a few meters) can already create a sufficient change in geometry to allow the float position solution to quickly reach a good precision, down to the level of a few centimeters.

2. Fine Carrier Frequency Offset Estimation

As the time-variant clock error is included in $\hat{\tilde{\delta}}_r^p(t_2)$ (cf. (25)), one can estimate the residual CFO based on a series of $\hat{\tilde{\delta}}_r^p(t_2)$. Given a $T_D = 1$ ms update interval of the position solution, we assume that the CFO is constant not only within one OFDM symbol, but also during the transmission period for the following analysis. Therefore, according to (25) and (15), one has

$$\hat{\tilde{\delta}}_r^p(kT_D) - \hat{\tilde{\delta}}_r^p\left((k-1)T_D\right) = \hat{\tilde{\vartheta}}_a(kT_D) - \hat{\tilde{\vartheta}}_a((k-1)T_D) \approx 2\pi\Delta\hat{\tilde{f}}_c(kT_D)T_D, \tag{28}$$

where

$$\Delta\tilde{f}_D(kT_D) = \Delta f_c(kT_D) - \Delta\check{f}_c(kT_D). \tag{29}$$

As the residual CFO is estimated based on $\tilde{\delta}_r^p(t_2)$ through the carrier phase-based positioning model, the range of the residual CFO is determined by the update rate of the relative clock error $\hat{\tilde{\delta}}_r^p(kT_D)$ (i.e., $\pm 1/2T_D$), and is much finer than the one using the shortened Moose's symbol, which depends on the subcarrier spacing (i.e., $\pm\Delta f$). Thus, combining the coarsely estimated CFO $\Delta\check{f}_c$, based on the shortened Moose's symbol, with the fine CFO estimate $\Delta\hat{\tilde{f}}_c$, the ultimate CFO is given by

$$\Delta\hat{f}_c(kT_D) = \Delta\check{f}_c(kT_D) + \Delta\hat{\tilde{f}}_c(kT_D). \tag{30}$$

V. EXPERIMENTAL RESULTS

An outdoor experiment has been carried out to assess the positioning performance of the SuperGPS system, using the carrier phase estimated through the OFDM burst ranging signal.

1. Experimental Setup

As presented in [6], each transmitter and the receiver is implemented based on the Ettus X310 Universal Software Radio Peripheral (USRP), which supports a maximum sampling frequency of 200 MSps with an effective bandwidth of 160 MHz. Time-frequency reference signals, in the form of a 10 MHz and 1 PPS are generated by a central atomic clock, which is located at VSL (the Dutch national metrology institute), a few kilometers away, and distributed to so-called timing nodes of the SuperGPS demonstration system on-site through an existing optical network. By connecting the USRPs to the timing nodes, which extract the time and frequency reference signals from the optical fiber, all radio transmitters in the SuperGPS system are synchronized at the 100 picoseconds level. The ranging burst signal for each transmitter occupies a time-slot of 21.6 microseconds as shown in Fig. 1.

In this project, the frequency band with a central carrier f_c at a frequency of 3960 MHz and a bandwidth of 160 MHz has been licensed for experiments and demonstration of the proof-of-concept of the SuperGPS system. In practice, other available central frequencies can be used, and it may not be necessary to occupy a contiguous band of 160 MHz [15]. It should be noticed that with a higher carrier frequency, the carrier phase becomes more sensitive to errors, as the same small offset or displacement will cause a larger phase rotation, which could be larger than one cycle and potentially lead to a cycle-slip.

The test site is located at The Green Village, which is a living outdoor lab on the TU Delft campus. Six transmitters are installed in lampposts along the road in an area of about 20-by-50 meters. Fig. 2(a) shows the layout of the experimental positioning system. The position of each transmitter antenna has been determined by using a land-surveying Total Station. The receiver was moved along a track of about 17 m forth and back, and the experiment lasted for about 71 seconds (while driving very slowly).

In the experiment, the receiver antenna is mounted on the roof of a ground-based vehicle as shown in Fig. 2(b). In addition, two 360-degree optical prisms are also mounted sideways on the vehicle, and they are tracked separately by two robotized Total Stations to reconstruct the ground truth values for the receiver. In this way, the ground-truth positions of the moving receiver antenna can be reconstructed, and used to evaluate the positioning performance of the SuperGPS system.

Due to the limitation of the existing infrastructure at the test-site, for example the height of the lamppost is generally about 3.5 meters above the ground, and given the height of the vehicle (about 2 meters), there is little height difference among different transmitters and the receiver. Consequently, the position-precision in the vertical direction will be poor. However, the ground
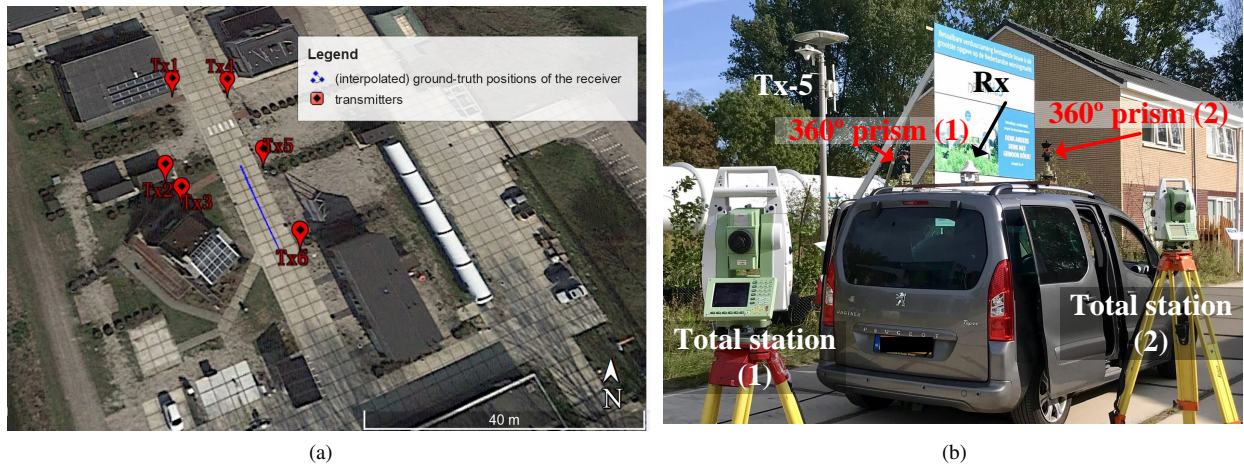
Figure 2: (a) Layout for the transmitters, trajectory of the interpolated ground-truth for the receiver (in blue), at The Green Village (photo from Google Earth) (b) the receiver antenna is mounted on the roof of a car, and two $360°$ optical prisms are also mounted sideways on this vehicle. Two prisms are tracked separately by two Total Stations to interpolate the ground-truth of the moving receiver.

vehicle generally moves smoothly on a straight and flat road without a significant variation in the vertical direction in this experiment. Therefore, a 2D positioning scenario is considered in this paper, and the height of the receiver antenna is measured by the Total Station, and assumed to be known a priori.
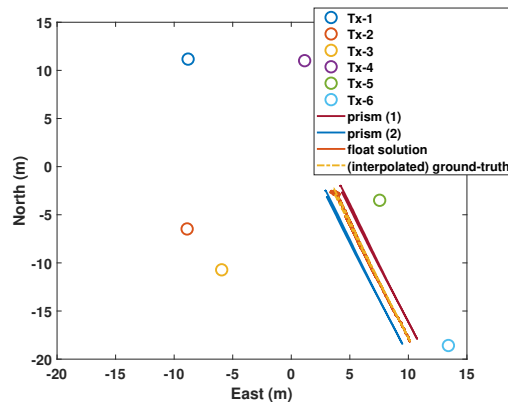
Figure 3: 2D positioning geometry, the interpolated trajectories of the two prisms and the moving receiver.

The 2D positioning geometry of the test site is presented in Fig. 3, and the horizontal dilution of precision (HDoP) values are typically around 1. To track a moving prism, the Total Station measures the angle and the distance with an update rate typically between 1 Hz to 10 Hz. In order to provide the ground truth with the same update rate of the position solutions (i.e., 1 kHz), interpolation is required for the location of the prisms. Here, a piece-wise linear least-squares estimation (LSE) with a moving window over 5 points, is applied to estimate the offset and the slope. Afterwards, the locations of the prisms are interpolated based on the linear model determined by piece-wise linear LSE with an update rate of 1 kHz. The interpolated trajectories of the two prisms are shown in Fig. 3.

Once the trajectories of the prisms are determined, one can reconstruct the trajectory of the receiver antenna. However, the two Total Stations shown in Fig. 2(b) are not synchronized in time. Cross-correlation between the time series of the trajectories of the two prisms is applied to determined the time lag. After aligning the trajectories in time, one can estimate the corresponding location of the receiver antenna, as the distances between the prisms and the receiver antenna are determined a priori. The interpolated ground-truth of the receiver antenna is also shown in Fig. 3 by a yellow dashed line.

2. Coarse Frequency Offset Estimation

As presented in section II., the rotation of the carrier phase is caused not only by the movement of the receiver (i.e., Doppler frequency offset), but also by the CFO. Generally, the CFO is much larger than the Doppler frequency offset. In the current SuperGPS system, the burst signal packet is used for ranging. If the phase rotation is more than a cycle within the transmission period, a cycle slip will occur in carrier phase tracking. To avoid such an issue, the CFO can be coarsely estimated and compensated based on the shortened Moose's symbol, as explained in equations (13)-(15).

Assuming that the CFO does not vary significantly within a certain period (e.g., a few seconds), the CFO is estimated for every received Moose's symbol in the received packets within 1 second, and its mean value over this 1 second time span is used to compensate the CFO for the received signal packets in the next second.
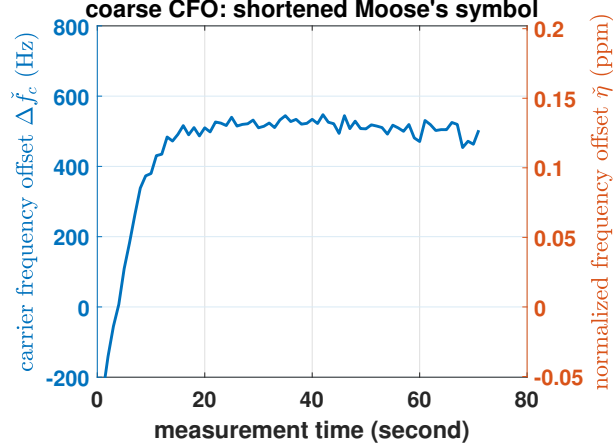

Figure 4: Coarse CFO estimates $\Delta \check{f}_c$ based on the shortened Moose's symbol and shown on the left vertical-axis, with an update interval of 1 second. As the transmission period T_D of each transmitter is 1 ms as shown in Fig.1(a), and there are 6 transmitters in the current prototype system, 6000 packets are used for coarse CFO estimation. The coarse CFO is determined by averaging over 6000 estimates per second. In addition, based on (3), the equivalent normalized frequency offset $\check{\eta}$ is shown on the right vertical-axis with a unit of ppm.

Fig. 4 shows the averaged coarse CFO estimates based on the shortened Moose's symbol, with an update rate of 1 Hz. After powering on the receiver device (i.e., USRP), it requires about 20 seconds to provide a relatively stable carrier frequency f'_c. The CFO is about 500 Hz and is much larger than the Doppler frequency offset, which, for example, is about 293 Hz when the receiver moves with a speed of 80 km/h. Therefore, it becomes necessary to compensate the CFO before estimating the carrier phase for positioning, so that any cycle slip can be avoided when using the burst ranging signal for carrier phase tracking.

Equivalently, the normalized frequency offset $\check{\eta}$ is computed based on the coarse CFO estimate $\Delta \check{f}_c$ (c.f. (3)), and also presented in Fig. 4 at the right vertical-axis. According to the results, the normalized frequency offset η is generally less than 1 ppm, which validates the assumption used in (4).

3. Positioning Performance

After compensating the coarsely estimated CFO in the received signal packets, the carrier phase is estimated based on (20) for all transmitters, where only the LoS path is considered in the design matrix $A(\tau)$. The unwrapped carrier phase, in which only the initial carrier phase ambiguity is preserved, is shown in Fig. 5(a). Although the CFO has been coarsely compensated, the residual CFO still dominates the change in the carrier phase (while the car drove only about 17 meters, the change in the carrier phase went up to 60 meter).

In addition, Fig. 5(b) shows the formal standard deviation versus the measurement time (i.e., $t_2 - t_1$), which evaluates the impact of the positioning geometry on the performance of the solutions in (24). Here, for simplicity, the SNR is assumed to be 10 dB for all transmitters. The variance matrix Q_φ is determined by (27), and consequently the formal standard deviation is determined by the square root of the formal error $Q_{\hat{u}}$ (26).

The formal standard deviation converges to a sub-centimeter level after about 20 seconds, during which the car had moved 1.77 m in East direction and 4.57 m in North direction, which creates a sufficient change in the geometry. Here the *averaged* formal standard deviation is computed for the position solution and the relative clock error, for measurement times larger than 20 seconds. The averaged standard deviation of the position solution in East and North direction are 0.2 cm and 0.17 cm, respectively, and 5.6×10^{-3} cycle for the relative clock error $\tilde{\delta}_r^p(t_1)$.
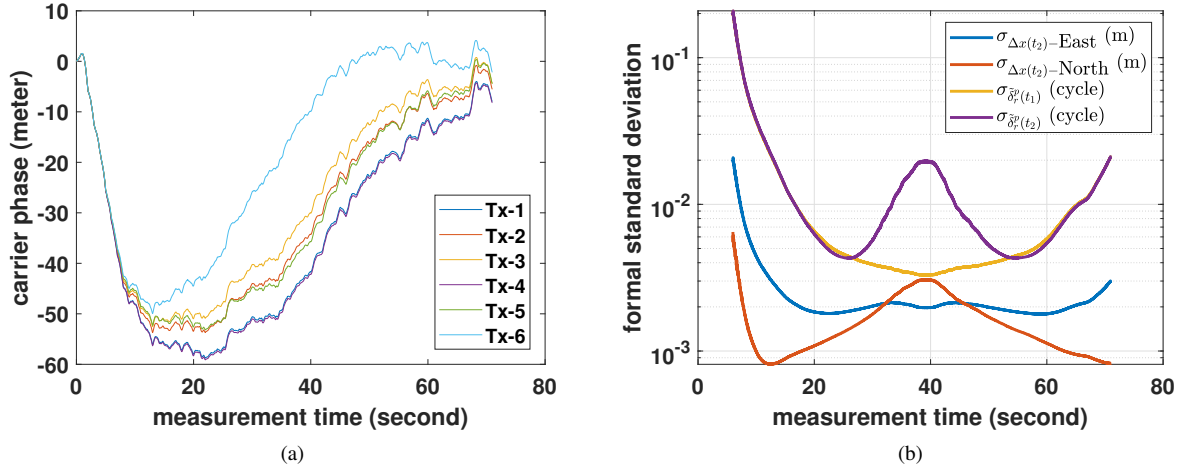
Figure 5: (a) Unwrapped carrier phase measurement in unit of length. As the receiver runs on its own clock, the change of the carrier phase is caused by the clock error, and the movement of the receiver, (b) formal standard derivations of the position solution in East and North direction $\sigma_{\Delta x(t_2)}$ (in m), the relative clock error $\sigma_{\tilde{\delta}_r^p(t_1)}$ and $\sigma_{\tilde{\delta}_r^p(t_2)}$ (in cycle).

As presented in section IV., the carrier phase estimated for two different time epochs with a change in geometry, is required to avoid rank deficiency in the positioning model (24). Two epochs of carrier phase measurements are used, where t_1 is kept fixed all the time to the starting epoch of the experiment, and epoch t_2 will be varied, up to 71 seconds past t_1 (i.e., t_2 can be replaced by kT_D, where k denotes the packet index).

By solving the positioning model (24), in which Tx-1 is selected as the pivot transmitter (i.e., $p = 1$), the position solutions and the interpolated ground truth values are presented in Fig. 6(a). To evaluate the positioning performance, the difference between the interpolated ground truth and position solution is computed and referred to as the position error. The position errors in the North and East direction are presented in Fig. 6(b). At the beginning of the experiment, the position solution has a large error and is poorly estimated, because there is only a little change in geometry. As time elapses, the difference between t_2 and t_1 in (24) gets bigger.
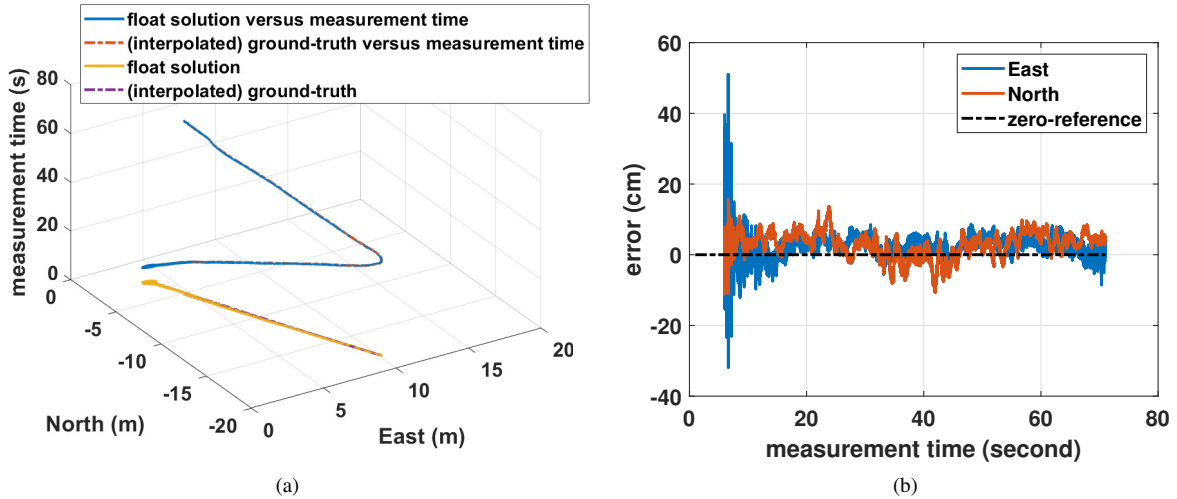

Figure 6: (a) 2D float position solutions in the East and North direction and the interpolated ground truth, (b) the position error versus the measurement time in the East and North direction.

Based on the experimental results shown in Fig. 6, the root-mean-square error (RMSE) of the float position solution in the

North-direction and the East-direction are 4.22 cm and 4.63 cm, respectively. It should be noted that these figures include the uncertainty in measuring the ground-truth with the Total Station, for instance identifying the phase center of the antenna for both the transmitters and the receiver (as shown in Fig. 2(b)) which has a height of 13.8 cm and a diameter of 16.75 cm.

The empirical mean, the empirical standard deviation of the position error, and the RMSE, for the measurement time larger than 20 second, are shown in Table. 1. Due to the uncertainty of the measured ground-truth, the empirical standard deviation of the position error is slightly larger than the formal standard deviation of the position solution shown in Fig. 5(b).

4. Fine Frequency Offset Estimation

Fig. 7 shows the relative clock error $\tilde{\delta}_r^p(t)$ which contains the ambiguity of the pivot transmitter Tx-1. As the carrier phase measurement for the first epoch (i.e., at t_1 in (24)) is kept the same in the positioning model as time elapses, the clock error $\tilde{\delta}_r^p(t_1)$ should be a constant value. As shown in Fig. 7(a), with a little change in geometry, at the beginning there are relatively large errors in the estimates of the clock error $\hat{\tilde{\delta}}_r^p(t_1)$. However, it converges after about 20 seconds, as the ground vehicle is continuously moving which improves the geometry. Fig. 7(b) shows the relative clock error $\hat{\tilde{\delta}}_r^p(t_2)$. Each time only two epochs of measurements are used for positioning, t_1 and t_2 in (24), where the second epoch t_2 (i.e., kT_D) is varied from taken close to t_1 to about 71 seconds later. The change of $\hat{\tilde{\delta}}_r^p(t_2)$ is caused by the change of the clock error (i.e., the residual CFO).
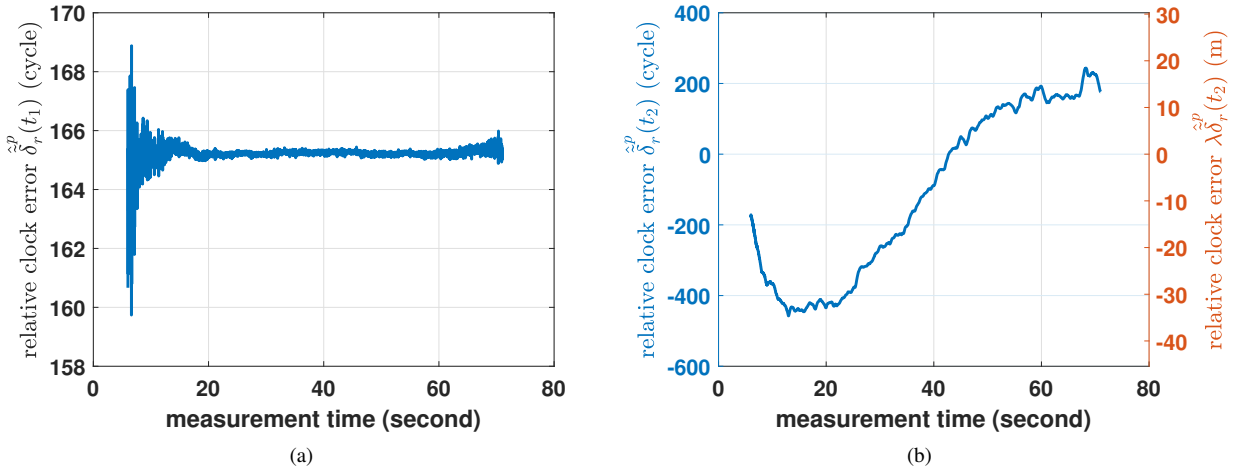

Figure 7: (a) Relative clock error $\hat{\tilde{\delta}}_r^p(t_1)$ for the first epoch of the pivot transmitter Tx-1, (b) relative clock error $\hat{\tilde{\delta}}_r^p(t_2)$ of Tx-1.

Here, the empirical standard deviation is also computed for the relative clock error $\hat{\tilde{\delta}}_r^p(t_1)$, when the measurement time is larger than 20 seconds. As shown in Table. 1, the empirical standard deviation of the relative clock error is 0.65 cm, which is close to the formal standard deviation as shown in Fig. 5(b), and indicates the quality of the carrier phase measurements.

Table 1: Empirical mean value and empirical standard deviation of the position error in East and North direction, and the relative clock error, as well as 2D position RMSE, based on the 51000 estimates when the measurement time $t_2 - t_1 \geq 20$ seconds in (24) (i.e., 51 second measurements with an update interval $T_D = 1$ ms).

unit: cm	(empirical) mean	(empirical) std.	RMSE
position error-East	2.64	2.06	3.52
position error-North	2.06	3.57	4.12
relative clock error $(\lambda \hat{\tilde{\delta}}_r^p(t_1))$	n/a	0.65	n/a

Using (28), Fig. 8(a) shows the fine CFO estimate $\Delta \hat{f}_c$ based on the clock error obtained in the positioning model. Similarly, due to a limited change in geometry, there are relatively large errors at the beginning. Then, using (30), Fig. 8(b) shows the CFO $\Delta \hat{f}_c(kT_D)$ constructed from the coarse CFO using the shortened Moose's symbol and the fine CFO using the carrier phase-based positioning model with an update interval of $T_D = 1$ ms, which can be used for frequency synchronization. This provides a better precision than only using the shortened Moose's symbol.
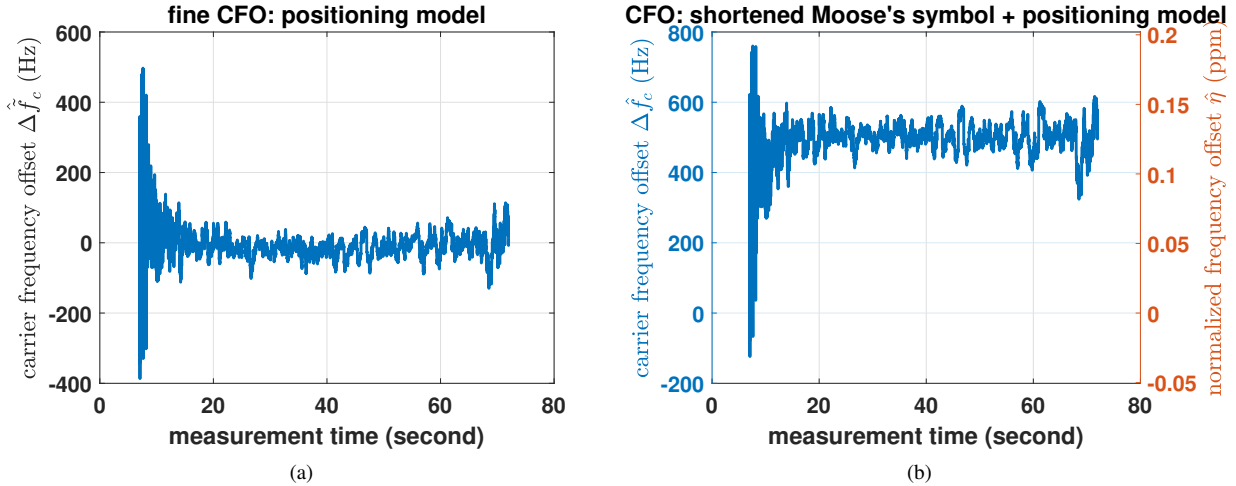
Figure 8: (a) Fine CFO estimate $\Delta\hat{\tilde{f}}_c$ based on the positioning model, (b) ultimate CFO estimate $\Delta\hat{f}_c$, which is the sum of the coarse CFO estimate based on the shortened Moose's symbol $\Delta\check{f}_c$ and the fine CFO estimate, with an update interval of $T_D = 1$ ms.

VI.   CONCLUSION

This paper presents the carrier phase-based positioning performance in a terrestrial positioning system, in which all transmitters are tightly synchronized through optically distributed time and frequency reference signals. As each transmitter uses a burst packet as the ranging signal, the carrier phase cannot be continuously tracked. To avoid cycle slips between transmission periods, the carrier frequency offset (CFO) is coarsely estimated and compensated based on the shortened Moose-symbol. Next, based on the carrier phase, a positioning model is proposed using the measurements acquired at two time epochs, which should have different geometry, and in which the carrier phase cycle ambiguities are kept as float numbers due to the uncalibrated initial phase offset in the transmitters. According to the experimental results, when the transmitters are densely deployed within a small area, the accuracy of the float position solutions converges to centimeter level within a short period of time. In addition, the clock error, which is computed along with the position solutions in the positioning model, can be used for fine CFO estimation and frequency synchronization. Using the carrier phase, the proposed SuperGPS terrestrial positioning system supports precise positioning with a centimeter level accuracy.

ACKNOWLEDGEMENT

REFERENCES

[1] J. Barnes, C. Rizos, J. Wang, D. Small, G. Voigt, and N. Gambale, "Locata: A new positioning technology for high precision indoor and outdoor positioning," in *Proceedings 2003 International Symposium on GPS/GNSS*, pp. 9–18, 2003.

[2] C. Rizos and L. Yang, "Background and recent advances in the locata terrestrial positioning and timing technology," *Sensors*, vol. 19, no. 8, p. 1821, 2019.

[3] X. Guo, Y. Zhou, J. Wang, K. Liu, and C. Liu, "Precise point positioning for ground-based navigation systems without accurate time synchronization," *GPS Solutions*, vol. 22, no. 2, p. 34, 2018.

[4] A. Alarifi, A. Al-Salman, M. Alsaleh, A. Alnafessah, S. Al-Hadhrami, M. A. Al-Ammar, and H. S. Al-Khalifa, "Ultra wideband indoor positioning technologies: Analysis and recent advances," *Sensors*, vol. 16, no. 5, p. 707, 2016.

[5] S. Gezici, Z. Tian, G. B. Giannakis, H. Kobayashi, A. F. Molisch, H. V. Poor, and Z. Sahinoglu, "Localization via ultra-wideband radios: a look at positioning aspects for future sensor networks," *IEEE Signal Processing Magazine*, vol. 22, no. 4, pp. 70–84, 2005.

[6] C. Diouf, H. Dun, T. Kazaz, G. Janssen, and C. Tiberius, "Demonstration of a decimeter-level accurate hybrid optical-wireless terrestrial positioning system," in *Proceedings of the 33rd International Technical Meeting of the Satellite Division of The Institute of Navigation (ION GNSS+ 2020)*, pp. 2220–2228, ION-Inst. of Navigation, 2020.

[7] E. F. Dierikx, A. E. Wallin, T. Fordell, J. Myyry, P. Koponen, M. Merimaa, T. J. Pinkert, J. C. Koelemeij, H. Z. Peek, and R. Smets, "White rabbit precision time protocol on long-distance fiber links," *IEEE Transactions on Ultrasonics, Ferroelectrics, and Frequency Control*, vol. 63, no. 7, pp. 945–952, 2016.

[8] P. Moreira, J. Serrano, T. Wlostowski, P. Loschmidt, and G. Gaderer, "White rabbit: Sub-nanosecond timing distribution over ethernet," in *2009 International Symposium on Precision Clock Synchronization for Measurement, Control and Communication*, pp. 1–5, IEEE, 2009.

[9] D. Vasisht, S. Kumar, and D. Katabi, "Decimeter-level localization with a single WiFi access point," in *13th USENIX Symposium on Networked Systems Design and Implementation*, pp. 165–178, 2016.

[10] K. Shamaei, J. Khalife, and Z. M. Kassas, "Exploiting LTE signals for navigation: Theory to implementation," *IEEE Transactions on Wireless Communications*, vol. 17, no. 4, pp. 2173–2189, 2018.

[11] J. A. Del Peral-Rosado, J. A. Lopez-Salcedo, F. Zanier, and G. Seco-Granados, "Position accuracy of joint time-delay and channel estimators in LTE networks," *IEEE Access*, vol. 6, pp. 25185–25199, 2018.

[12] A. Abdallah, K. Shamaei, and Z. M. Kassas, "Assessing real 5G signals for opportunistic navigation," in *Proceedings of the 33rd International Technical Meeting of the Satellite Division of The Institute of Navigation (ION GNSS+ 2020)*, pp. 2548–2559, ION-Inst. of Navigation, 2020.

[13] P. Wang and J. Morton, "Carrier phase tracking architecture for positioning in LTE networks under channel fading conditions," in *Proceedings of the 33rd International Technical Meeting of the Satellite Division of The Institute of Navigation (ION GNSS+ 2020)*, pp. 2605–2617, ION-Inst. of Navigation, 2020.

[14] C. Yang, L. Chen, O. Julien, S. Andrey, and R. Chen, "Carrier phase tracking of OFDM-based DVB-T signals for precision ranging," in *Proceeding of the 30th International Technical Meeting of The Satellite Division of the Institute of Navigation (ION GNSS+ 2017)*, pp. 736–748, ION-Inst. of Navigation, 2017.

[15] H. Dun, C. Tiberius, C. Diouf, and G. Janssen, "Sparse signal bands selection for precise time-based ranging in terrestrial positioning," in *2020 IEEE/ION Position, Location and Navigation Symposium (PLANS)*, pp. 1372–1380, IEEE, 2020.

[16] H. Dun, C. Tiberius, and G. Janssen, "Positioning in a multipath channel using OFDM signals with carrier phase tracking," *IEEE Access*, vol. 8, pp. 13011–13028, 2020.

[17] G. H. Golub and V. Pereyra, "The differentiation of pseudo-inverses and nonlinear least squares problems whose variables separate," *SIAM Journal on Numerical Analysis*, vol. 10, no. 2, pp. 413–432, 1973.

[18] S. K. Wilson, "Synchornization," in *Orthogonal frequency division multiplexing for wireless communications* (Y. G. Li and G. L. Stuber, eds.), ch. 5, Springer, 2006.

[19] T. M. Schmidl and D. C. Cox, "Robust frequency and timing synchronization for OFDM," *IEEE Transactions on Communications*, vol. 45, no. 12, pp. 1613–1621, 1997.

[20] D. Tse and P. Viswanath, "Point-to-point communication:detection, diversity and channel uncertainty," in *Fundamentals of Wireless Communication*, ch. 3, pp. 64–142, Cambridge university press, 2005.

[21] I. F. Progri, M. C. Bromberg, and W. R. Michalson, "Maximum-likelihood GPS parameter estimation," *Navigation*, vol. 52, no. 4, pp. 229–238, 2005.

[22] S. Verhagen and P. Teunissen, "Least-squares estimation and kalman filtering," in *Springer handbook of Global Navigation Satellite Systems* (P. Teunissen and O. Montenbruck, eds.), ch. 22, Springer, 2017.

[23] W. Baarda, "S-transformations and criterion matrices," *Netherlands geodetic commission*, 1973.